Available online at www.sciencedirect.com

SciVerse ScienceDirect

Journal of the European Ceramic Society 32 (2012) 2633–2639

www.elsevier.com/locate/jeurceramsoc

The densification and strength of porous Y-TZP materials with a bimodal particle size distribution for dental applications

Sebastjan Perko [a,*], Ales Dakskobler [a,b], Tomaz Kosmac [a,b]

[a] *Josef Stefan Institute, Engineering Ceramics Department, Jamova 39, SI-1000 Ljubljana, Slovenia*
[b] *Center of Excellence, Namaste, Ljubljana, Slovenia*

Available online 6 March 2012

Abstract

In this study the densification behavior of bimodal Y-TZP powder compacts consisting of nano/sub-micron-sized particles was studied and an explanation for their improved flexural strength while biscuit-sintered is provided. An in situ-heating TEM analysis revealed that up to 800 °C only the nanoparticles sinter in a bimodal mixture without any densification. By increasing the temperature to 900 °C the densification of the nanoparticles begins and partially densified nanoparticle clusters migrate into the contact area between the core particles. Consequently, the driving force for the sintering of the powder-blend compacts is reduced and this is reflected in a slower densification compared to that of the core material. At 1000 °C the sintered nanoparticle clusters begin to incorporate into the core material, resulting in a sharp increase in the strength due to the increased neck area. Biscuit-sintered powder-blend compacts reached a plateau of strength at 670 MPa, which was reached at a relative density of 70%.

Keywords: Sintering; Electron microscopy; ZrO_2; Biomedical applications; Densification

1. Introduction

In recent decades there have been major advances in the application of sintered yttria partially stabilized zirconia (Y-TZP) ceramics for load-bearing applications in restorative dentistry. One of the emerging problems pertaining to Y-TZP for dental applications is associated with its high elastic modulus relative to that of dentin, as this may lead to the development of stresses at the interface of the zirconia frameworks and the tooth preparations. This can in turn cause a marginal seal failure due to fracture, leading to periodontal disease and secondary caries. The most straightforward approach in reducing the elastic mismatch is by sintering the powder compacts to a fixed degree of the densification. Well-established equations exist that can be used to describe the relationship between the porosity and the elastic moduli of biscuit-sintered Y-TZP.[1] In general, however, biscuit-sintered materials exhibit poor mechanical properties compared to their densely sintered counterparts.[2,3] It is the purpose of modern ceramic processing to better control both the particle packing during shaping as well as the microstructure during sintering, so that the consolidated samples contain fewer strength-determining pores/flaws.[4–6] Regarding the evolution of the microstructure during sintering, Hardy and Green[7] demonstrated that surface diffusion results in the formation of necks between particles during the initial stage of sintering, which governs the mechanical properties of biscuit-sintered materials. In order to improve the sintered strength of such moderately porous ceramic components, a mixing of ceramic slurries with different particle-size distributions was proposed.[8–10] To better control the distribution of the finer fraction in the powder mixture we can employ the aggregation method, i.e., hetero- or homo-aggregation, which can occur between particles differing in their size, shape, sign of charge and charge density.[11] By employing this approach, a homogeneous distribution of nanoparticles in a powder-blend material can be achieved.[12,13]

The mixing of coarse and relatively fine ceramic powders is a well-established and common method used to control the firing shrinkage.[14] It is well known that mixtures of this type can exhibit an increased green density, although this increase is often less than the theoretical prediction.[15] However, one of the consequences of mixing ceramic materials is a pronounced change in the sintering kinetics. For a bimodal powder mixture, the addition of fine particles in volume fractions greater than 30 vol% was found to control, i.e., to enhance, the densification,

* Corresponding author. Tel.: +386 14773940; fax: +386 14773171.
E-mail address: sebastjan.perko@ijs.si (S. Perko).

0955-2219/$ – see front matter © 2012 Elsevier Ltd. All rights reserved.
doi:10.1016/j.jeurceramsoc.2012.02.001

whereas for lower volume fractions of fine particles the coalescence of the coarser fraction will dominate.[16] The effect of the particle size distribution on the sintering of ceramics depends on how the particle size distribution is changed during the processing. Some studies have examined the effect of changing the standard deviation of the particle size distribution while keeping the median particle size constant. It has been found that wider particle size distributions lead to faster densification rates during an intermediate stage of sintering.[17] However, a narrower distribution may prolong the intermediate stage of sintering, resulting in a less pronounced grain coarsening during the final stage.[18] For bimodal distributions of WC–Co materials, for example, it was observed that the densification rate strongly depends on the size ratio of the mixture, allowing for both faster and slower shrinkage compared to monomodal packing.[19] Wonisch et al.[20] employed a discrete-element method that was used to investigate the relationship between the distribution of particle sizes and the macroscopic sintering behavior of ceramic powders. They found that an overall decrease in the densification rate should be expected when the width of the particle size distribution is increased.

In a previous investigation of ours,[21] we have reported on the slower densification of powder-blend Y-TZP material prepared using the core-shell approach. An increased flexural strength in the moderate porosity range compared to the biscuit-sintered core particles alone was also recorded and ascribed to an increased area of the interparticle contacts. In addition, with a further densification above 70% TD the strength remained essentially constant, which was tentatively attributed to the evolution of strength-determining flaws due to the coalescence of pores.

The purpose of the present work was to support this assumption by studying the densification behavior and superior flexural strength of biscuit-sintered Y-TZP powder-blend powder compacts. A homogeneous bimodal particle size distribution was used in which the coarser fraction dominated and the effect of the finer fraction's addition on the densification rate and the resultant strength of biscuit-sintered ceramics were evaluated. The difference in the relative density achieved with the powder blend compared to the core material was explained by combining the results of a dilatometric analysis and an in situ-heating TEM experiment. Finally, a 2D-SEM study was designed, aimed at monitoring the pore growth, which can be used to interpret the evolution of the strength-determining pores and flaws as well as the grain growth of the shell fraction.

2. Experimental

The starting materials used were submicron-sized zirconia powder TZ-3Y (Tosoh, Japan) and nano-sized zirconia powder, supplied in the form of an aqueous suspension (XZO 1356/01, Mel Chemicals, Manchester, UK). The submicron-sized powder is supplied in the form of granulated powder. Both materials contain 3 mol% of Y_2O_3 in the solid solution. The bimodal powder blend was prepared by wet-attrition milling of the submicron-sized core powder for 2 h in deionized water containing citric acid acting as a dispersant. After the milling step the suspension was washed and centrifuged to remove any residual citric acid. The sediment was re-dispersed in deionized water to obtain a 40 wt% suspension of core particles. Afterwards, the 17% of nanosized particles was added. The selected amount was needed to continuously cover the surface of the core particles. After stirring, a powder-blend suspension of the homogeneously distributed shell fraction attached to the surface of the core fraction was obtained. Exact information on the preparation of the starting materials is given elsewhere.[21] The samples of powder blend were wet-shaped by slip casting into plaster molds to produce pellets of 19 mm in diameter and 1.7 mm in height, and cylinders measuring 4 mm in diameter and 6 mm in height. The as-received nanoparticle slurry was shaped into cylinders, but not into pellets since the shaping of nanosized powders is still an unresolved issue. For the reference material the sub-micron-sized TZ-3YB powder supplied as a ready-to-press granulate was used. The same sample geometries, both pellets and cylinders, were prepared by dry-pressing. Dry-pressing was used in order to achieve the same green densities as in the case of the wet-shaped powder blend.

A contact-mode dilatometer (Bahr, Thermoanalyse) was used to monitor the densification of the cylinders during the constant rate of heating (CRH) for all three materials. The samples were sintered at heating and cooling rates of 5 °C/min up to the end temperature without any dwell time. The end temperature was 1200 °C for the nanoparticle compacts and 1500 °C for both the powder blend and the reference samples.

The pellets were subjected to the same sintering schedule, except that the isothermal stage was introduced in this case. The samples were divided into four groups and sintered in temperature intervals of 100 °C, starting at 1000 °C and finishing at 1400 °C. The sintering was carried out in an ambient air atmosphere at a heating rate of 5 °C/min and 2 h dwell time at the end temperatures (NABER, Germany).

The experimental work is summarized in Table 1.

The sintered density was measured using Archimedes' method with mercury as the immersion liquid. The biaxial flexural strength of the pellets was measured using a piston-on-three-balls test, at a loading rate of 1 mm/min (Instron 4301, UK). The fracture surfaces were examined using XRD analysis in order to verify the transformability of the material under externally applied stress. The powder mixtures for the in situ-heating TEM study were prepared using the same procedure as described above. The powder-blend sample for observation in the TEM was prepared on a platinum-sputtered, Ni-based, TEM grid. The maximum allowed temperature for the in situ TEM sintering is 1000 °C and that was the ultimate temperature. The experiment was conducted at a 5 °C/min heating rate and with a 1-h dwell time at the end temperature.

3. Results

Dilatometric curves obtained during the CRH experiments of the three powder compacts are shown in Fig. 1a. The specimens consisting of nanosized particles started to densify at 600 °C and they reached almost theoretical density at 1200 °C. The densification of the powder-blend and submicron-sized powder compacts started at 800 °C and 900 °C, respectively, and

Table 1
Summary of the experimental work.

	Shaping method	T treatment	T treatment
TZ-3YB	Dry-pressing, $\rho_g = 44\%$	Non-isothermal: 5 °C/min, $T_{end} = 1500$ °C	Isothermal stage 5 °C/min, $T_{end} = 1000$–1500 °C, $t_{dwell} = 2$ h
Nano Y-TZP	Slip casting, $\rho_g = 50\%$	Non-isothermal: 5 °C/min, $T_{end} = 1200$ °C	–
Powder blend	Slip casting, $\rho_g = 45\%$	Non-isothermal: 5 °C/min, $T_{end} = 1500$ °C	Isothermal stage 5 °C/min, $T_{end} = 1000$–1400 °C, $t_{dwell} = 2$ h

reached their final density at 1400 °C and 1450 °C, respectively. The most remarkable difference in the densification behavior among the three powder compacts occurs in the low-temperature region, i.e., between 600 °C and 800 °C, in which a slight densification is observed in the case of nanosized compacts, whereas the other two materials do not show any noticeable shrinkage. Fig. 1b shows the densification rate of these three materials. The nanosized powder compact evidently exhibits the highest densification rate and the lowest temperature at which the maximum densification rate is reached at 1050 °C. The other two materials shrink at a slower rate and reach the maximum rate of densification at 180 °C higher temperature, i.e., at 1230 °C. In the temperature interval between 800 °C and 1080 °C the powder-blend compact densifies at a higher rate compared to the sub-micron sized material.

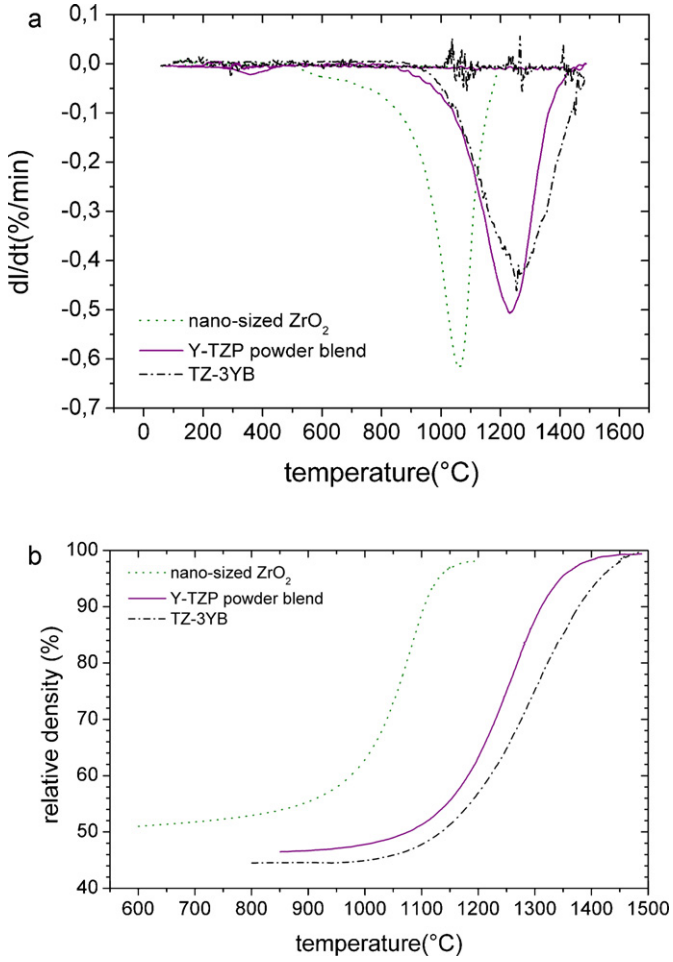

Fig. 1. (a) Dilatometric analysis. (b) Densification rate.

The relative densities of the powder compacts obtained after isothermal biscuit-sintering at various temperatures, but below those at which the ultimate density is reached, are shown in Fig. 2. The dry-pressed reference core material exhibits a faster densification with an almost linear increase of the relative density up to 1400 °C, where a material density of 99% is achieved. The powder-blend compacts exhibit a steady increase in the relative density up to 1100 °C and do not increase this noticeably when increasing the temperature to 1200 °C. From this temperature onwards the material densifies like the pure core material. The presence of nanoparticles in the powder blend hinders the densification of the core material.

In order to get a better insight into the densification behavior during isothermal sintering at lower temperatures, in situ-heating TEM experiments of the Y-TZP powder-blend material were performed. The dynamics of the events were first evidenced by successive TEM micrographs taken at different time intervals in the heating stage of 1000 °C. Fig. 3 shows the complete integration of a particular single nanoparticle that was initially adsorbed onto the core particle's surface during the 1 h dwelling time.

However, before the nanoparticles are "swallowed" by the larger core particles due to the Ostwald ripening mechanism some sintering between the nanosized particles will occur. As shown in Fig. 4a, these will start to sinter at 600 °C, forming clusters that at higher temperatures, such as 900 °C, literally move into the contact areas between the core particles (Fig. 4b).

We believe that a hindered densification of the powder blend, at the expense of neck formation during the isothermal biscuit-sintering, leads to an increased strength of the Y-TZP material

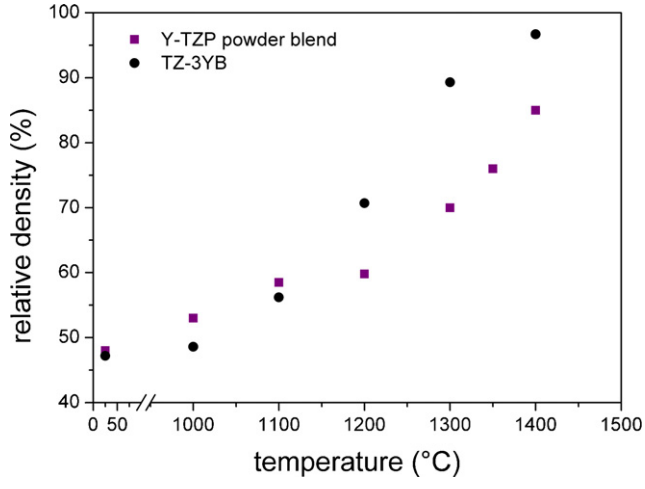

Fig. 2. Dependence of relative density on temperature for TZ-3YB and nanostructured Y-TZP materials.

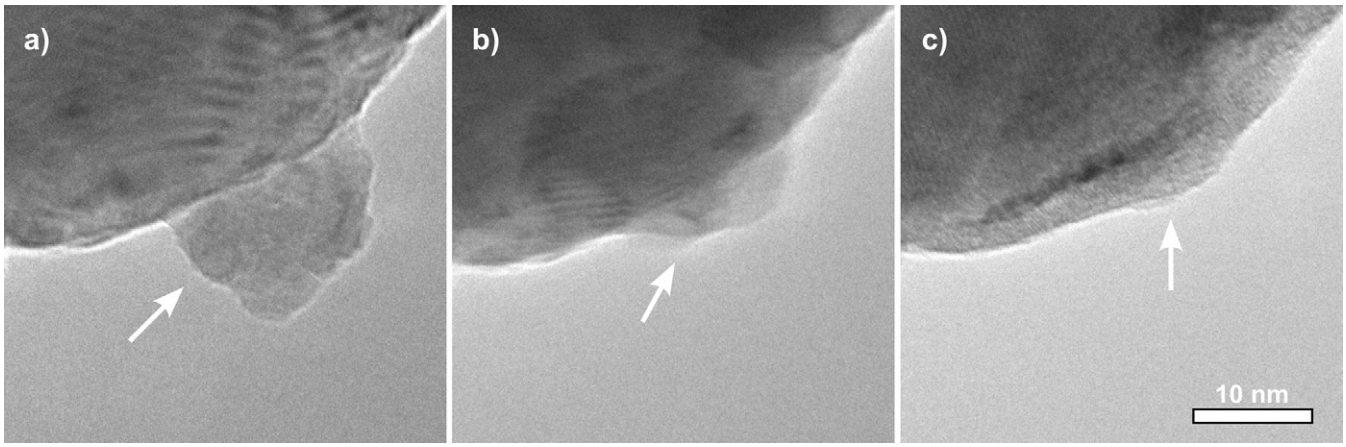

Fig. 3. In situ heating TEM study at 1000 °C showing a time sequence of nanoparticle incorporation into a core particle at (a) 30 min, (b) 40 min and (c) 60 min.

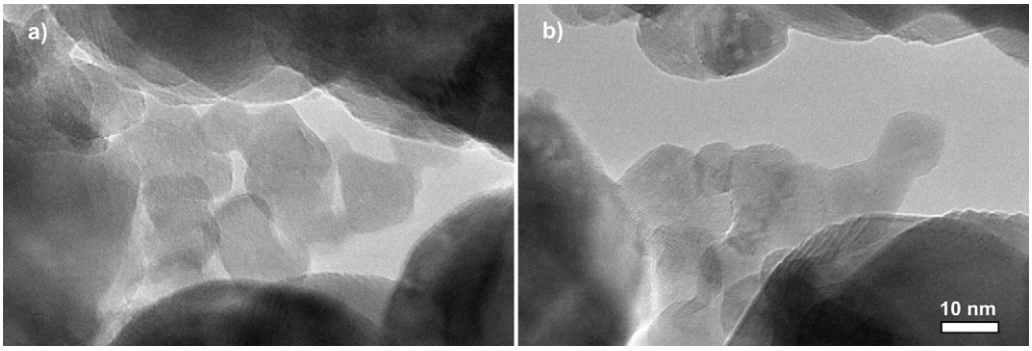

Fig. 4. In situ heating TEM study performed at (a) 600 °C where nanoparticles enter initial stage of sintering and (b) 900 °C showing movement of sintered nanoparticle cluster into the contact area between two core particles.

in the moderate porosity range (Fig. 5). Notice that a strong increase in the strength was achieved with minimal densification from 58% TD to 60% TD, by heating the samples to reach 70% of TD the peak strength value was recorded. From this point onwards the strength remains practically constant, but the standard deviation increases.

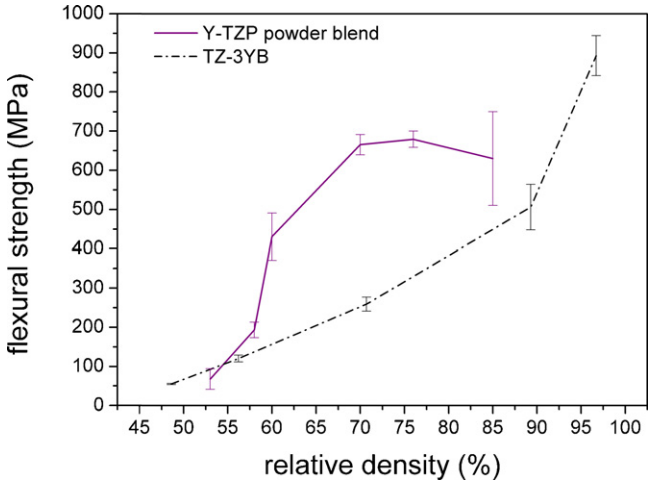

Fig. 5. Biaxial flexural strength vs. relative density for nanostructured ceramics along with a comparison curve of dry-pressed and biscuit-sintered TZ-3YB powder.

Fig. 6 shows characteristic X-ray diffraction patterns in the 25–40° 2θ range obtained from the fracture surface of the TZ-3YB and the powder blend ceramics, sintered for 2 h at 1200 °C, i.e., under sintering conditions yielding the highest strength of

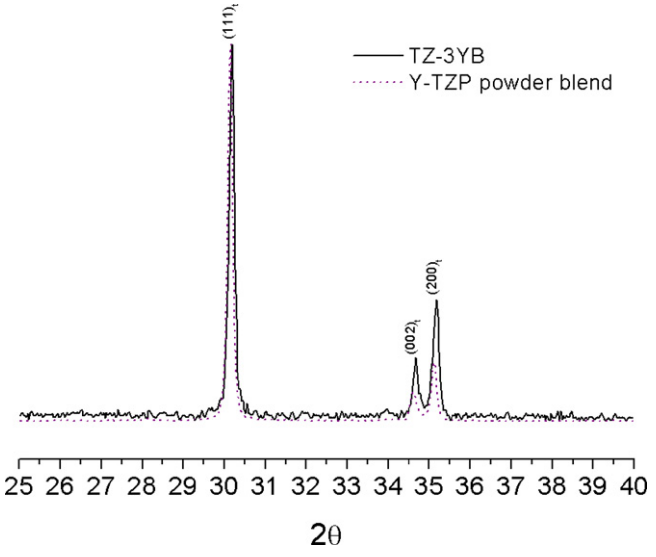

Fig. 6. XRD patterns obtained from fracture surfaces of TZ-3YB (black line) and powder blend ceramics (violet dotted line). (For interpretation of the references to color in this figure legend, the reader is referred to the web version of the article.)

powder blend samples. The pattern of both ceramics displays a sharp tetragonal (1 1 1) peak of high intensity at 2θ 30.2° and two less intensive peaks at 2θ 34.6° and 36.2° belonging to T(2 0 0) and T(0 0 2) reflections which are practically identical to the pattern obtained from the as-sintered surface indicating that no t–m transformation has taken place.

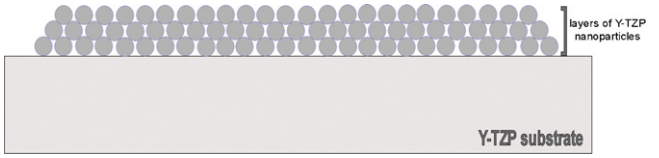

Fig. 7. Scheme of the 2D sintering experiment.

4. Discussion

The in situ-heating TEM study can be used to support the differing results on the densification behavior during CRH and isothermal sintering schedules. Two major observations enabled the phenomenological explanation of the densification behavior of the nanostructured material during both sintering schedules. First, the observed difference in the densification rate between the powder-blend and the reference core material during the CRH treatment in the temperature interval from 800 °C to 1080 °C, as shown in Fig. 1b, can be attributed to single nanoparticles that are positioned amid the core particles. These densify with the core particles, leading to a slightly larger shrinkage of the powder-blend samples compared to the pure core material. Fig. 3 indicates that in this case the volume diffusion dominates as an atomic transport mechanism between the nano- and the core particles, and in this way the initial discrepancy in the shrinkage rate is evidenced. Second, by increasing the end temperature gradually from 600 °C to 900 °C in 100 °C increments, only the nanoparticles are sinter-active and they form partially densified sintered clusters (Fig. 4a). During heating, and by introducing the dwell time into the sintering schedule, the sintered clusters gain enough time to move into the contact areas between the core particles, thereby reducing the curvature between them (Fig. 4b). The consequence of the migration is a reduced driving force for all the diffusion mechanisms occurring during the sintering of the core particles and the densification of the powder blend is impeded up to 1200 °C (Fig. 2).[22,23] At higher temperatures the beneficial effect of the nanoparticles is lost and the densification of the powder blend proceeds as in the case of the core powder compact. Fig. 4a and b also evidence the onset of the diffusion processes by forming necks between the nanoparticles at temperatures as low as 600 °C. At 900 °C the clustered nanoparticles bridge the core particles by forming a neck.

The data obtained from the in situ-heating TEM study led to the conclusion that the powder-blend material with a bimodal particle size distribution in the core-shell configuration represents a unique situation in sintering. As long as the activation energy of the coarser fraction is not overcome during heating, the particles of the finer fraction in contact will sinter to form clusters. During the dwell time step in the sintering schedule these will migrate into the contact areas between the core particles. As opposed to the dry-pressed core-powder compacts where necks are formed only between submicron-sized particles, in the case of the bimodal particle size distribution, the nanoparticles enable the formation of necks between nanosized and/or submicron-sized particles. These events increase the interparticle contact area in biscuit-sintered compacts exhibiting a TD of 70%. With further densification, the strength remains inevitably constant and this could be attributed to the evolution of strength-determining flaws due to the coalescence of pores. In order to better understand this, a simple sintering experiment was designed, aimed at monitoring the pore-size evolution responsible for the plateau in the flexural strength.

In this experiment a uniform distribution of the nanoparticles in the core-shell material was considered, as schematically shown in Fig. 7. The samples were prepared using nearly dense and thermally etched Y-TZP substrates of 20 mm diameter and 2 mm height. A drop of a highly diluted suspension of Y-TZP nanoparticles was applied to the substrate surface, which was subsequently dried at room temperature.

After drying, the samples were sintered at the same end-temperatures and dwell times as the bulk samples. The SEM micrographs taken from the surface of samples sintered from 1100 °C to 1300° are shown in Fig. 8b–d. Up to 1100 °C only minor grain growth can be seen, but no pore coalescence is observed (Fig. 8b).

At 1200 °C, in contrast, an extensive grain growth occurs, which is accompanied by a marked pore coalescence (Fig. 8c), whereas at 1300 °C the pores are already so large that they become strength determining. Assuming that a similar mechanism is operating in the bulk samples, it is likely that these large pores are responsible for the plateau of the flexural strength, shown in Fig. 8a. In the literature one can find statements that the pore size remains constant up to 83% of the relative density,[18] while others claim that along the grain growth the total number of pores will be reduced, but their average diameter and length will increase as a consequence of coalescence,[24] giving support to our results. Being fully aware of the effects of constrained sintering, the results are in agreement with the results on flexural strength.

With reference to results presented in Fig. 6, none of the biscuit sintered materials exhibited the stress-induced transformation. Both fracture surfaces consisted of tetragonal zirconia, without any trace of transformed monoclinic zirconia in the XRD pattern. It has been demonstrated that externally applied stress exerted by cutting, grinding, impact or fracture, is capable of generating significant t → m transformation of the zirconia grains.[25] This is evidenced by the occurrence of the characteristic M(1 1 $\bar{1}$) and M(1 1 1) peaks in the XRD pattern, commonly accompanied by the T(1 1 1) peak broadening and a reversed intensity of the tetragonal (0 0 2) (2 0 0) peaks at 2θ 34.6° and 36.2°. The absence of these characteristic features in the XRD pattern obtained from the fracture surfaces implies that that the two biscuit-sintered ceramics were un-transformable under an externally applied stress. Since there is a critical Y-TZP grain size below which the t–m transformation cannot be induced, it is likely to assume that during biscuit-sintering of our two materials

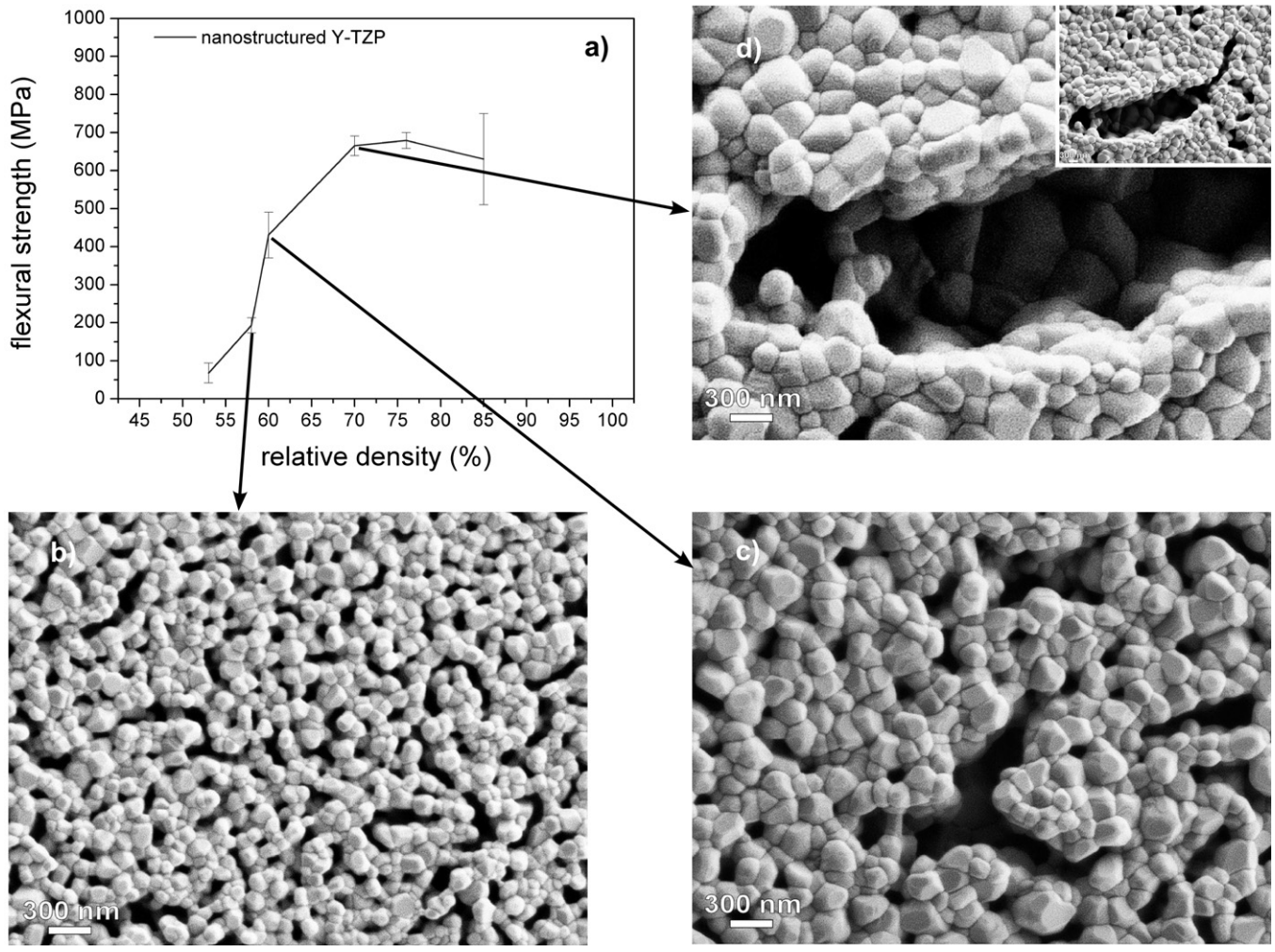

Fig. 8. SEM-based sintering study of pore growth in a 2D situation showing (a) flexural strength dependence on relative density and the corresponding samples sintered at (b) 1100 °C, (c) 1200 °C and (d) 1300 °C.

the grains have not yet grown to such an extent to reach the critical size for the stress-induced transformation. Being so, it is also not likely to expect any beneficial effect of the transformation toughening on the fracture toughness.[26]

5. Conclusions

The densification of the Y-TZP powder blend in a core-shell configuration is reduced compared to the sub-micron-sized core material during isothermal biscuit-sintering. This was due to the reduced curvature between the core particles, caused by the nanoparticles that fill the neck areas between them during sintering. At the same time, an enhanced neck growth resulted in a higher strength in the moderate porosity range. During the constant rate of heating (CRH) treatment, in contrast, these phenomena were not observed because the crucial stage of retarded densification, i.e., the migration of nanoparticles into the neck area between coarser particles, did not occur. Although our 2D SEM model does not take into account the effects of constrained sintering, we believe that from the sintering experiment of the nano-sized powder spread onto the sintered Y-TZP substrate it can be concluded that a plateau of strength is reached due to the evolution of the strength-determining flaws by extensive pore growth.

Acknowledgments

The financial support from the Center of Excellence Nanocenter Ljubljana, funded by the European Regional Development Fund is gratefully acknowledged. The authors also gratefully acknowledge Dr. Andraž Kocjan and Dr. Irena Pribošič for performing the SEM and in situ heating TEM analyses, respectively.

References

1. Luo J, Stevens R. Porosity-dependence of elastic moduli and hardness of 3Y-TZP ceramics. *Ceram Int* 1999;**25**:281–6.
2. Deng ZY, Yang JF, Beppu Y, Ando M, Ohji T. *J Am Ceram Soc* 2002;**85**:1961–5.
3. Kosmac T, Andrzejczuk M, Kurzydlowski KJ. *Ceram Eng Sci Proc* 2008;**27**(2).
4. Lange FF. Powder processing science and technology for increased reliability. *J Am Ceram Soc* 1989;**72**.

5. Aksay IA, Lange FF, Davis BI. Uniformity of Al_2O–ZrO_2 composites by colloidal filtration. *J Am Ceram Soc* 1983;**66**:C190–2.
6. Lange FF. Shape forming of ceramic powders by manipulating the interparticle pair potential. *Chem Eng Sci* 2001;**56**:3011–20.
7. Hardy D, Green DJ. Mechanical properties of partially sintered alumina. *J Eur Ceram Soc* 1995;**15**:769–75.
8. Li G, Jiang Z, Jiang A, Zhang L. *Nanostruct Mater* 1997;**8**(6): 749–54.
9. Kritikaki A, Tsetsekou A. Fabrication of porous alumina ceramics from powder mixtures with sol–gel derived nanometer alumina: effect of mixing method. *J Eur Ceram Soc* 2009;**29**:1603–11.
10. Tari G, Ferreira JMF, Fonseca AT, Lyckfeldt O. Influence of particle size distribution on colloidal processing of alumina. *J Eur Ceram Soc* 1998;**18**:249–53.
11. Caruso F. Nanoengineering of particle surfaces. *Adv Mater* 2001;**13**: 11–22.
12. Cerbelaud M, Videcoq A, Abelard P, Pagnoux C, Rossignol F, Ferrando R. *Langmuir* 2008;**24**:3001–8.
13. Wu Q, Wang Z, Kong X, Gu X, Xue G. A facile strategy for controlling the self assembly of nanocomposite particles based on colloidal steric stabilization theory. *Langmuir* 2008;**24**:7778–84.
14. Schmidt SA, Nettleship I. The effect of coarse particles on the microstructural evolution of porous alumina sintered at 1375 °C. *J Eur Ceram Soc* 2004;**24**:2741–7.
15. Messing GL, Onoda GY. Inhomogeneity-packing density relations in binary powders. *J Am Ceram Soc* 1978;**61**:1–5.
16. Smith JP, Messing GL. Sintering of bimodally distributed alumina powders. *J Am Ceram Soc* 1984;**67**:238–42.
17. Yeh TS, Sacks MD. Effect of particle size distribution on the sintering of alumina. *J Am Ceram Soc* 1988;**71**:C484–7.
18. Shiau FS, Fang TT, Leu TH. Effect of particle-size distribution on the microstructural evolution in the intermediate stage of sintering. *J Am Ceram Soc* 1997;**80**:286–90.
19. Petersson A, Agren J. Sintering shrinkage of WC–Co materials with bimodal grain size distibutions. *Acta Mater* 2005;**54**:111–8.
20. Wonisch A, Kraft T, Moseler M, Riedel H. Effect of different particle size distributions on solid-state sintering: a microscopic approach. *J Am Ceram Soc* 2009;**92**:1428–34.
21. Perko S, Dakskobler A, Kosmac T. High-performance nanostructured ceramics. *J Am Ceram Soc* 2010.
22. Ashby MF. A first report on sintering diagrams. *Acta Metall* 1974;**22**:275–89.
23. Swinkels FB, Ashby MF. A second report on sintering diagrams. *Acta Metall* 1981;**29**:259–81.
24. Rosolowski JH, Greskovich C. Theory of the dependence of densification on grain growth during intermediate stage sintering. *J Am Ceram Soc* 1974;**58**:177–82.
25. Reddy KM, Mukhopadhyay A, Basu B. Microstructure–mechanical–tribological property correlation of multistage spark plasma sintered tetragonal ZrO2. *J Eur Ceram Soc* 2010;**30**:3363–75.
26. Basu B. Toughening of yttria-stabilised tetragonal zirconia ceramics. *Int Mater Rev* 2005;**50**:239–56.